Metrol. Meas. Syst., Vol. 25 (2018) No. 2, pp. 387–402.

PAN POLSKA AKADEMIA NAUK

METROLOGY AND MEASUREMENT SYSTEMS

Index 330930, ISSN 0860-8229

www.metrology.pg.gda.pl

M&MS

APPLICATION OF POLY-HARMONIC SIGNALS TO EDDY-CURRENT METAL DETECTORS AND TO ADVANCED CLASSIFICATION OF METALS

Jakub Svatoš, Tomáš Pospíšil, Josef Vedral

Czech Technical University in Prague, Department of Measurement, Prague 6, Technická 2, 16627, Czech Republic
(✉ *svatoja1@fel.cvut.cz*, +420 224 352 201, *pospito7@fel.cvut.cz*, *vedral@fel.cvut.cz*)

Abstract

A limited ability to discriminate between different materials is the fundamental problem with all conventional eddy-current-based metal detectors. This paper presents the use, evaluation and classification of non-traditional excitation signals for eddy-current metal detectors to improve their detection and discrimination ability. The presented multi-frequency excitation signals are as follows: a step sweep sine wave, a linear frequency sweep and sin(x)/x signals. All signals are evaluated in the frequency domain. Amplitude and phase spectra and polar graphs of the detector output signal are used for classification and discrimination of the tested objects. Four different classifiers are presented. The classification results obtained with the use of poly-harmonic signals are compared with those obtained with a classical single-tone method. Multi-frequency signals provide more detailed information, due to the response function – the frequency characteristic of a detected object, than standard single-tone methods. Based on the measurements and analysis, a metal object can be better distinguished than when using a single-tone method.

Keywords: eddy current, metal detector, poly-harmonic signal, signal processing, classification.

1. Introduction

The metal detection together with distinguishing different metals is the essential part of many branches – security, industry, ecology, archaeology or humanitarian demining [1]. Metal detectors are used in airports or important buildings as walk-through metal detectors to improve security. They are widely used in pharmacy, food and chemical industries or by the military for a land clearance from anti-tank or antipersonnel mines [2]. Amateur treasure hunters or archaeologists use detectors to detect ancient artefacts and old coins [3]. Last but not least, metal detectors are used for humanitarian demining [4, 5], where a handheld metal detector plays the key role during demining of *Explosive Remnants of Wars* (ERW).

There are many methods of metal detection [6], but the electromagnetic detectors (Eddy-current-based metal detectors) are still the most commonly used types of metal detectors, although they have their weaknesses. Such detectors poorly recognize or discriminate different materials or objects [7]. These detectors, used nowadays, usually work with a single-tone signal detecting the changes of phase and amplitude of a measured signal (*Very Low Frequencies detectors*) or monitoring the time delay of a measured pulse (*Pulse Induction detectors*) to estimate the

Article history: received on Dec. 21, 2017; accepted on Mar. 10, 2018; available online on Jun. 30, 2018, DOI: 10.24425/119564.

presence of a metal object with different conductivity or permeability. It leads to a limited discrimination ability, because some types of metals or objects have similar responses. For example, if a detector operator looks for a specific material (*e.g.* gold), the response can be mistaken for a material that has a similar response (*e.g.* tinfoil) [8]. The operating frequency of a detector is a very important parameter. The frequency influences the depth of penetration of the eddy current, as well as resolution and sensitivity. Low-frequency magnetic fields penetrating deeper into the ground are less affected by magnetic or mineralized soils and the skin effect is reduced. On the other hand, high frequencies offer better resolution and sensitivity. Thus, the detector discrimination and detection qualities strongly depend on the frequency of an excitation signal. It enables to explore poly-harmonic signals and their processing and classification, to detect and to better identify an object, unlike conventional single-tone methods [9].

There are several papers presenting analyses and use of multi-frequency signals for eddy-current metal sensors. These eddy-current sensors are usually used for non-destructive testing or metal separation. The majority of papers deal with the change of the sensor coil impedance [10, 11] or use the magnetic induction spectroscopy [12].

Applying multi-harmonic or poly-harmonic signals and their processing offers an improvement to the determination ability of eddy-current metal detectors. Due to multiple frequencies of excitation signals, the response – frequency characteristic of a detected material is acquired in a wide band. In this frequency characteristic, multiple phases and amplitudes carry information about the detected object, and more detailed information about the object than that obtained with a standard single-tone method. The spectrum of the poly-harmonic signal is suitable for further spectral analysis of the response function (for more details of the response function see [9, 13]) of the detected object. The response function can be used for discrimination of the object and its classification into a selected class.

The paper presents three non-conventional poly-harmonic excitation signals, their processing, evaluation and classification. These signals are as follows: step sweep sinusoidal, linear frequency sweep sinusoidal and sinc signals. The emphasis is put primarily on the sinc signal. *Support Vector Machine classifier* (SVC) together with *Naive Bayes* (naivebc), *k-Nearest Neighbours* (KNN) and *Linear Nearest Mean Classifier* (NMC) are used for classifying. This paper continues the previous experiments published in [9, 14] and [15], presents new approaches to the measured signal processing and is supplemented with new results. A possible classification of objects into classes is also presented.

2. Methods

Three different excitation poly-harmonic signals: a step sweep sine-wave signal, a linear frequency sweep signal and a sine cardinal (sinc) signal, were evaluated. The experimental measurements were performed in the frequency domain. All the presented experimental data were measured with a search head of a Schiebel ATMID metal detector [16, 17]. The detector uses a double D configuration of the searching head with a diameter of 260 mm. The numbers of turns of transmitting (*Tx*) and receiving (*Rx*) coils were 17 and approx. 190, respectively. The electrical equivalent circuit of the coil is shown in Fig. 1.

R_1 is a resistance (ohms) and L_1 is an inductance of *Tx* coil, R_2 is a resistance, L_2 is an inductance of *Rx* coil, and L_{1-2} corresponds to the mutual inductance between coils. The T–shape configuration of inductances in Fig. 1 corresponds to a transformer with inductances L_1 of the primary and L_2 of secondary windings and the mutual inductance L_{1-2} between both windings. The measured parameter values for an operating frequency of 8.17 kHz are listed in

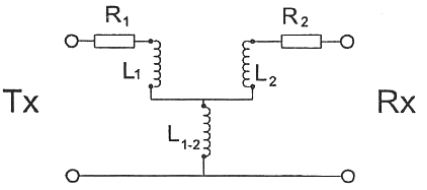

Fig. 1. A diagram of the equivalent circuit of ATMID coil.

Table 1. These parameter values correspond to the parameter values given by the manufacturer [17]. The resonant frequency of the transmitting coil is approx. 90 kHz, whereas of the receiving coil – approx. 45 kHz. Since the usable frequency range for poly-harmonic signals has to be below the resonant frequencies of both coils, the frequency of excitation signal has been set to a range of 1 kHz to 30 kHz.

Table 1. Double-D coil parameter values for the operating frequency of 8.170 kHz.

R_1 (Ω)	L_1 (mH)	R_2 (Ω)	L_2 (mH)	L_{1-2} (μH)
1.2	0.774	182	3.35	0.1

If only the search head, without its electronic, is used and if it operates on different frequencies than the tuned/balanced frequency (8.17 kHz), the coils will become unbalanced and the output voltage will not be minimal due to the mutual inductance L_{1-2}. This effect can be used for further signal processing to compare the signal from a tested target with the signal without any target present – caused solely by the mutual inductance L_{1-2}. Fig. 2 shows a block diagram of the measurement setup. The setup consists of a 14-bit programmable function generator AFG 3102, a 15-bit digitizer connected to a PC and a Signal Recovery 7265 lock-in amplifier.

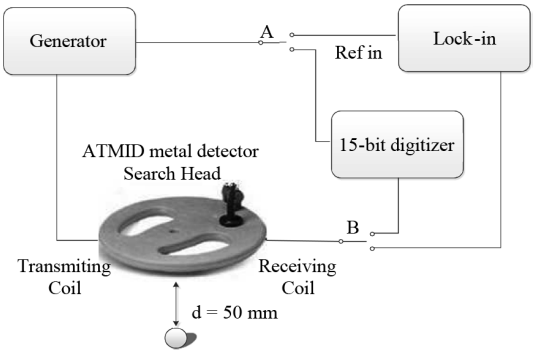

Fig. 2. A block diagram of the measurement setup.

For measuring linear frequency sweep sinusoidal and sinc signals, switches A and B are switched to the 15-bit digitizer. In the case of the step sweep excitation signal the keys are switched to Lock-in. The detector operates on a non-magnetic platform in a laboratory without any background noise. All excitation signals are 10 V voltage signals. As specimens, homogenous spheres of different diameters made of different ferrous and non-ferrous materials were used. These targets were placed on the axis of the greatest sensitivity of the search head in the open air at the distance of 50 mm from the coils. The targets were not placed into the ground

to avoid the ground effect [18]. The measured data were processed in MATLAB software with classification pattern recognition PRTools ver. 5 [19]. In the frequency domain, amplitude and phase spectra were calculated and presented together with polar graphs.

2.1. Step sweep sine-wave signal

The frequency step sweep signal, which consists of multiple frequencies equally stepped from lower to higher frequencies can be used to measure and verify the behaviour of the object response function. An AFG 3102 generator generates measured frequencies of the voltage excitation signal from 3 kHz to 25 kHz with a step of 2 kHz. The frequency range covers one decade of the response function for each target. The signal from the receiving coil is measured by the Signal Recovery 7265 lock-in amplifier. As a reference signal for the lock-in amplifier, the same signal attenuated to the amplitude of 1 V (due to the lock-in reference input channel restrictions) is used (Fig. 2).

2.2. Linear frequency sweep signal

The linear frequency sweep, or the chirp signal, is commonly used in many areas, *e.g.* audio applications, radar and sonar systems or communications [20]. Its advantage, as of all poly-harmonic signals, is that it can cover a wide frequency range of the response function. As a disadvantage, the impossibility of using synchronous demodulation has to be considered. Signals composed of multiple frequencies have to be first digitized and then processed using an advanced signal processing method. The chirp signal spectrum is a rectangular function beginning with frequency f_0 and ending with frequency f_1. The linear frequency sweep signal is generated using the formula:

$$u(t) = \sin\left[2\pi\left(f_0 + \frac{k}{2}t\right)t\right] \qquad \text{and} \qquad k = \frac{f_1 - f_0}{T}, \tag{1}$$

where f_0 is a starting (initial) frequency; f_1 is a stopping frequency; t is a sweep time and k is a sweep rate. The selected starting frequency is 3 kHz and the sweep time is 10 ms. The signal from the receiving coil is acquired by a 15-bit analogue-to-digital converter with the sampling frequency of 1 MS/s (Fig. 2). The signals that are composed of multiple frequencies, have to be first digitized. After digitizing, advanced signal processing can be performed. The measured data are filtered by a bandpass FIR filter of 300^{th} order and Blackman-Harris window has been used. The lower frequency of the band pass filter is $f_d = 1$ kHz and the upper frequency – $f_h = 30$ kHz. *Discrete Fourier Transformations* (DFTs) from the filtered signals were calculated with a *Fast Fourier Transform* (FFT) algorithm. FFT was calculated for $N = 1048578$, which is the nearest power of two for 1 M samples (1000 periods with 1000 samples each). Although the coherent sampling cannot be done, the results are relevant because of a large number N of samples used in signal processing.

2.3. Sin(x)/x

The sine cardinal signal, commonly referred to as the sinc function, is one of the poly-harmonic signals suitable for metal detector excitation to cover a wide range of the response functions of the detected object. The sinc signal is a very prospective and widely used excitation signal due to its spectrum [21, 22]. The sinc function spectrum is appropriate for further spectral analysis of the response function of the detected object. The number and positions of spectral

lines can be easily defined and set. Another advantage is that all frequencies are applied at once. A modified sinc signal, which is used in the experiments, is composed of two sinc signals with the same parameters, where the second half of the period is inverted (Fig. 3). One period of the signal is described by the formula:

$$u(t) = H\left(t + \frac{T_1}{2}\right)\left[\frac{\sin\left(\frac{2\cdot\pi\cdot t}{T_2}\right)}{\frac{2\cdot\pi\cdot t}{T_2}}\right] - H\left(t - \frac{T_1}{2}\right)\left[\frac{\sin\left(\frac{2\cdot\pi\cdot t}{T_2}\right)}{\frac{2\cdot\pi\cdot t}{T_2}}\right], \tag{2}$$

where H is a Heaviside function, which chops the segment of the sinc function in a defined time range $\langle -T_{1/2},\ T_{1/2}\rangle$. The following parameters describe the used modified sinc signal: frequencies $f_1 = 1/T_1 = 0.5$ kHz, $f_2 = 1/T_2 = 10$ kHz, 10 significant carrier frequencies and an amplitude of 10 V. The repeating frequency of $f_R = 1$ kHz and significant frequencies at each 2 kHz result from these parameters.

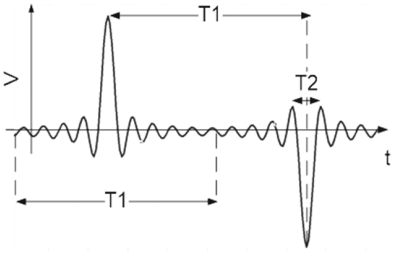

Fig. 3. A time plot of the modified sinc signal.

The generator was externally synchronized via the synchronization output of the digitizer (Fig. 2). To ensure the repeatability of the sinc signal generation, the digitizer was triggered by TTL signal from the generator. The 15-bit analogue-to-digital converter measured the signal with the sampling frequency of 1 MS/s. The record was one second long. First, the background signal without the presence of any tested object caused only by the mutual inductance L_{1-2} was measured. This signal was compared with signals corresponding to the tested spheres. The amplitude and phase spectra obtained using the Fourier transformation were presented. Firstly, the signal was filtered by the same FIR filter. These filtered signals were then processed by DFT using an FFT algorithm, and were calculated from the number of samples $N = 1048578$, which is the nearest power of two for 1 M samples.

3. Results

Materials measured in all the experiments and used for classification were brass, bronze, INOX AISI 316, INOX AISI 420 and 52100 100Cr6. Spheres with diameters $d = 10$ mm, 12 mm, 15 mm, 20 mm and 25 mm were used. These materials were selected as the representative ones of ferrous and non-ferrous materials. An overview of electromagnetic properties of the selected materials is given in Table 2. The real and imaginary parts and the amplitude and phase spectra of the measured signal, as well as polar graphs, were considered. The polar graphs can be used for a better interpretation of the detected objects and subjective discrimination by the operator.

Table 2. Electromagnetic properties of the selected materials.

Material	Conductivity σ (Sm^{-1})	Relative permeability μ_r (–)
brass	1.500	1
bronze	0.740	1
INOX AISI 316	0.137	1.02
INOX AISI 420	0.139	600
52100 100Cr6	0.465	300

3.1. Step sweep sine-wave signal

Examples of one ferrous (AISI 52100 100Cr6) and one non-ferrous (bronze) spheres of diameters of 10 mm and 20 mm are presented. The frequency dependency of amplitude and phase of the received signal is presented in the following figures (Fig. 4 – AISI 52100 100Cr6 material and Fig. 5 – bronze material). In the magnitude chart (Fig. 4a), it is evident that the induced voltage increases with increasing frequency and diameter of the spheres equally. The greater differences between induced voltages are noticeable at higher frequencies. The inductive limit [8] for a smaller diameter is reached sooner than for a greater diameter and the increase of amplitude becomes smaller. The phase chart (Fig. 4b) shows expected results. The absolute phase shift increases with the diameter of the target. It confirms that the chrome steel sphere, as a ferrous material, can shift the phase value from positive to negative [9].

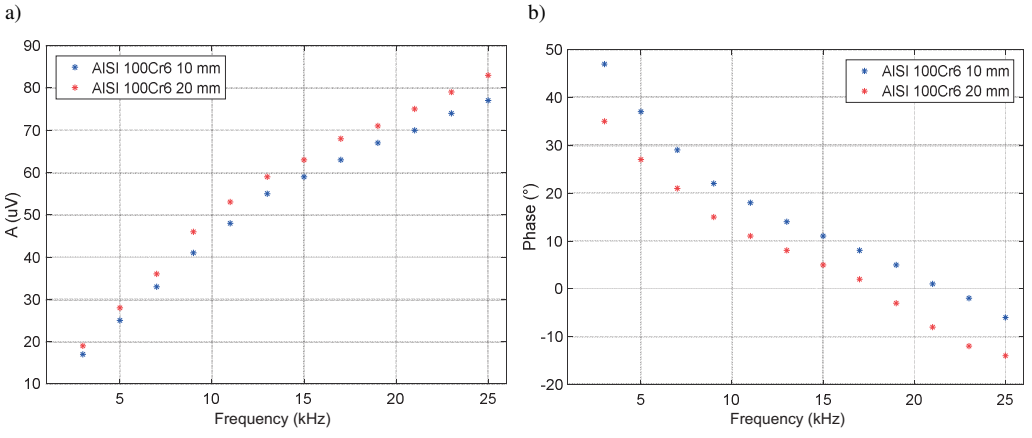

Fig. 4. The magnitude (a) and phase (b) of AISI 52100 100Cr6 spheres with diameters of 10 mm and 20 mm.

Bronze spheres of diameters 10 mm and 20 mm are presented as non-ferrous material. The obtained results are shown in Fig. 5. The induced voltage increases with increasing frequency. The phase shift of only bronze spheres goes to negative values, unlike that of ferrous steels. It corresponds to the theory concerning ferrous and non-ferrous materials. The phase shift increases more with a diameter at lower frequencies, but decreases with increasing frequency while it also changes less significantly. It is caused by the inductive limit.

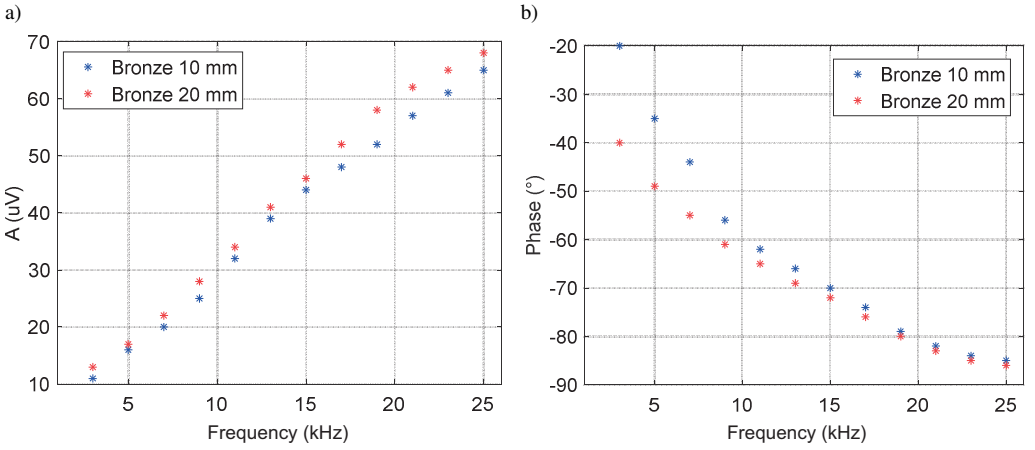

Fig. 5. The magnitude (a) and phase (b) of bronze spheres with diameters of 10 mm and 20 mm.

3.2. Linear frequency sweep signal

The amplitude and phase spectra of a ferrous AISI 52100 100Cr6 sphere with a diameter of 10 mm and a non-ferrous bronze sphere with the same diameter of 10 mm are presented. The phase spectra were calculated and corrected as the difference between the transmitted and received signal phase spectra. Figs. 6 and 7 show the amplitude and phase spectra as well as a polar graph of two materials. They show the processed data of AISI 52100 100Cr6 and bronze spheres (both spheres with a diameter of 10 mm), respectively.

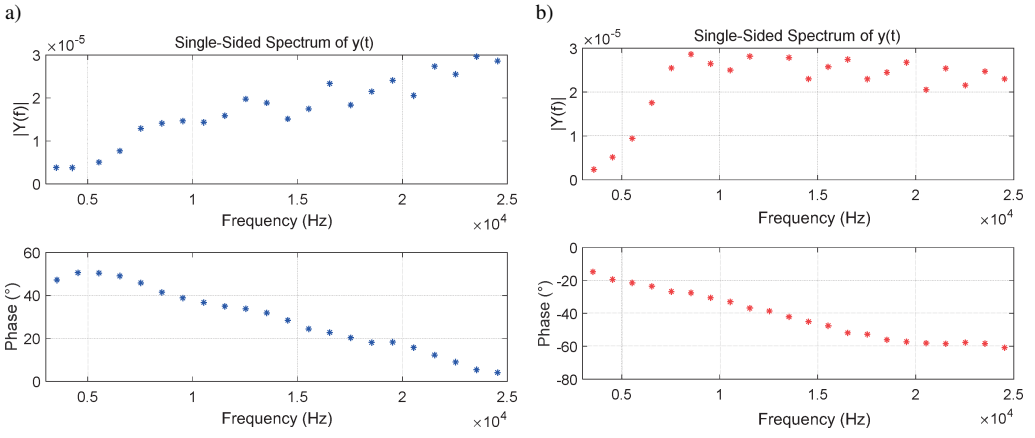

Fig. 6. The amplitude and phase spectra of AISI 52100 100Cr6 sphere with a diameter of 10 mm (a); The amplitude and phase spectra of a bronze sphere with a diameter of 10 mm (b).

The shape of amplitude spectra for both materials shows that the material with a higher relative permeability induces a higher voltage, especially at higher frequencies. It corresponds to the step sweep sine-wave results and also to the theory. However, a noticeable difference is visible for the measured data of a bronze sphere where the magnitude for higher frequencies (greater

than 10 kHz) does not increase. It can be explained by a very low level of the received signal and/or reaching the inductive limit by the induced voltage. The phase spectra of both materials confirm what is to be expected; the ferromagnetic materials, which have a relative permeability higher than one, have the phase shift from positive to negative values and the non-ferromagnetic materials have only negative values of the phase shift. The polar graph presented in Fig. 7 shows comparisons of both materials.

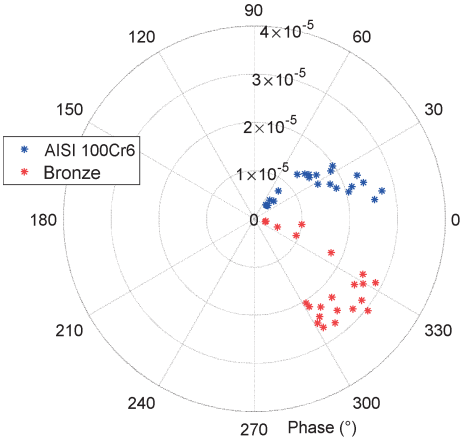

Fig. 7. A polar graph of both measured spheres.

3.3. Sin(x)/x

The presented materials are ferrous AISI 52100 100Cr6 and INOX AISI 420, whereas non-ferrous materials are brass and bronze. The phase spectra were calculated from the definition of a complex variable. All presented phase spectra were calculated as the difference between the phase spectrum of the signal, which corresponds to the measurement without any target (mutual inductance L_{1-2}, no object) and the phase spectrum of the signal, which corresponds to the measurement with a testing target. For better presentation and comparison, the spectra of compared signals shown in the following figures are shifted by ± 100 Hz. It is done only for better demonstration only. Figs. 8 and 9 show the measured amplitude and phase spectra together with a polar graph of ferromagnetic AISI 52100 100Cr6 and INOX AISI 420 testing spheres of two different sizes (diameters of 10 mm and 20 mm).

The amplitude spectrum (Fig. 8a), which corresponds to AISI 52100 100Cr6 material, is greater at all frequencies than the amplitude spectrum of the signal, which corresponds to the absence of any object. It is caused by the ferrous material permeability, which is much greater than one. In general, the magnitude spectra become higher for all ferrous materials with increasing the sphere diameter. Magnitudes for low frequencies increase more significantly than those for higher frequencies, which can be caused by the character of the response function. The phase shift difference confirms that ferrous materials shift the phase from positive to negative values. For a greater diameter, the absolute phase shift is increasing, whereas the relative phase shift is decreasing due to reaching closer to the inductive limit.

The next presented ferromagnetic object (Fig. 9) is stainless steel INOX AISI 420, which has similar electromagnetic properties as chrome steel 100Cr6. The amplitude and phase spectra

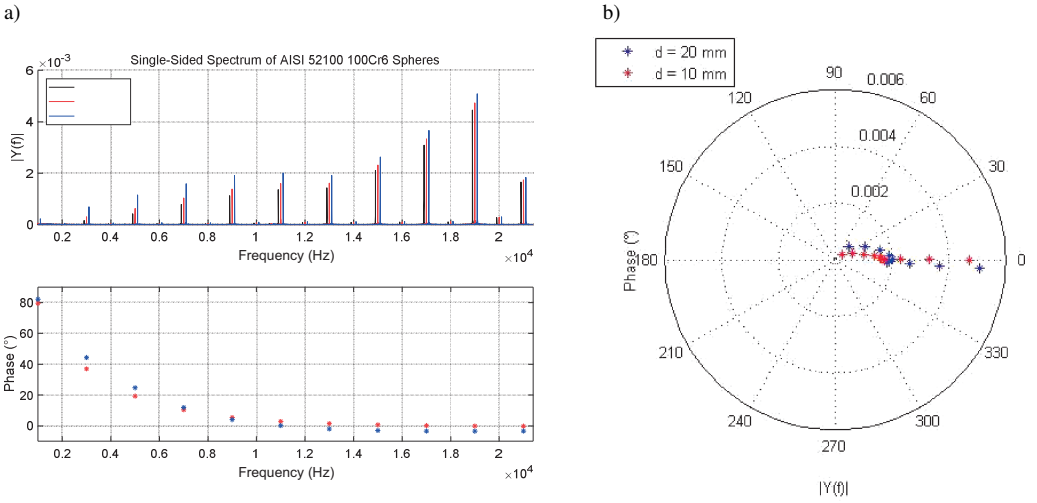

Fig. 8. The amplitude and phase spectra (a) and a polar graph (b) corresponding to AISI 52100 100Cr6 spheres with diameters of 10 mm and 20 mm.

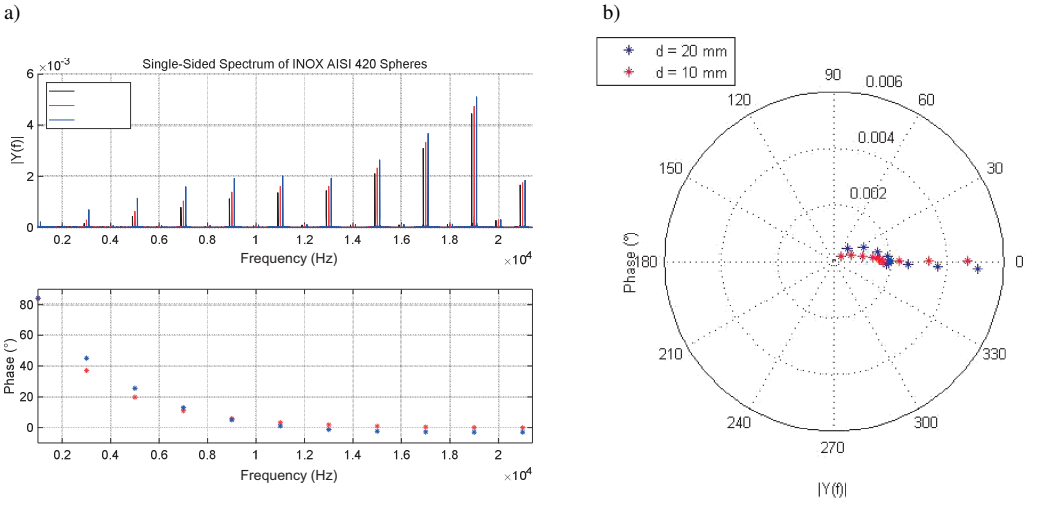

Fig. 9. The amplitude and phase spectra (a) and a polar graph (b) corresponding to INOX AISI 420 spheres with diameters of 10 mm and 20 mm.

are similar, too. Not surprisingly, at lower frequencies, the amplitude spectrum of the signal that corresponds to the INOX AISI 420 sphere increases more than at higher frequencies, similarly as for the 100Cr6 chrome steel sphere. The phase difference spectrum also shows the same trend. The first presented non-ferrous material is brass. Brass spheres with diameters of 10 mm and 20 mm are presented in Fig. 10.

The amplitude spectrum shows an essential difference from the ferrous materials. At higher frequencies, non-ferrous materials cause a suppression of the induced voltage and a drop in spectral lines. A similar situation emerges with the difference of phase spectra. As expected, the

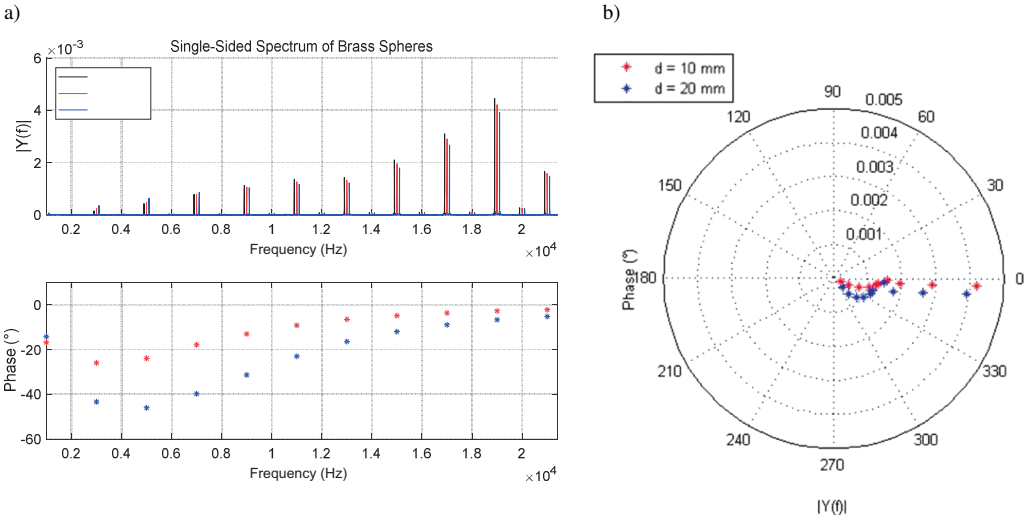

Fig. 10. The amplitude and phase spectra (a) and a polar graph (b) corresponding to brass spheres with diameters of 10 mm and 20 mm.

phase shift caused by the non-ferrous objects goes only to negative values. At lower frequencies, the phase difference between the signal, which corresponds to the non-ferrous material, and the signal, which corresponds to the measurement without any target present, is greater, as a diameter of the sphere becomes greater. At higher frequencies, a similar situation as for ferrous material occurs in the way that the relative phase shift decreases, reaching the inductive limit. The absolute phase shift becomes greater with a greater diameter of spheres. In Fig. 11, non-ferrous bronze material is presented.

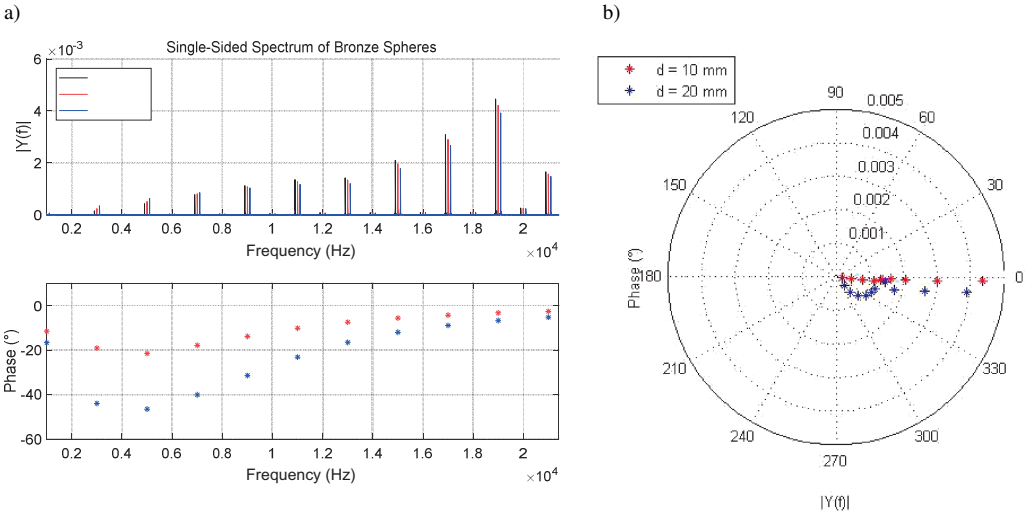

Fig. 11. The amplitude and phase spectra (a) and a polar graph (b) corresponding to bronze spheres with diameters of 10 mm and 20 mm.

The results resemble the situation for different ferrous materials. The response of non-ferrous materials – bronze and brass – is similar to each other. The behaviour of the amplitude and even the phase spectra is similar. The response function changed minimally because both materials have a similar conductivity. A more detailed comparison of similar ferrous and non-ferrous materials is presented in Fig. 12.

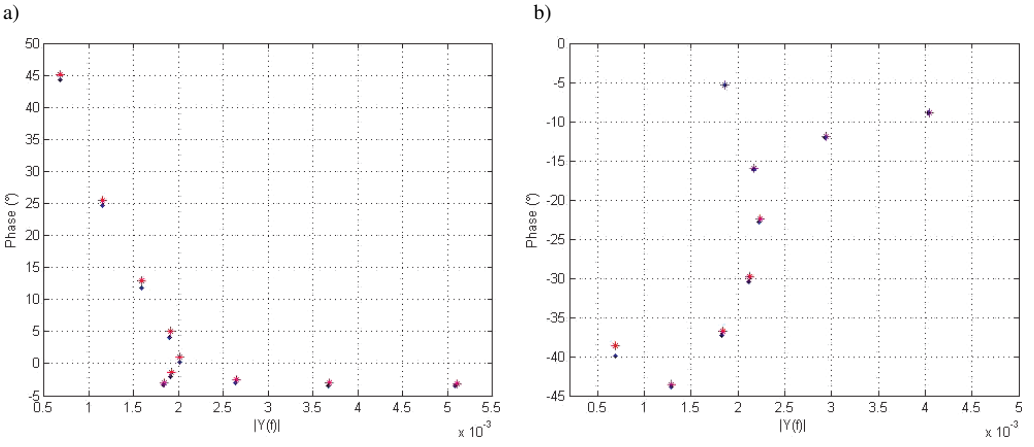

Fig. 12. An X-Y chart corresponding to INOX AISI 420 and AISI 52100 100Cr6 spheres with diameters of 20 mm (a) and an X-Y chart corresponding to brass and bronze spheres with diameters of 20 mm (b).

Figure 12a shows the relation (X-Y chart, x-axis ~magnitude, y-axis ~phase) between the amplitude and phase spectra involving two specimens of similar materials: INOX AISI 420 and AISI 52100 100Cr6 spheres with diameters of 20 mm. The phase difference corresponding to these materials is slightly greater than 1 degree at lower magnitudes (corresponding to lower frequencies) and slightly smaller than 1 degree at higher magnitudes (corresponding to higher frequencies). The difference between both materials follows the trend of the phase spectrum. The minimal difference between the amplitude spectra is caused by a similar response parameter α value which depends on conductivity and on a relative permeability of the material [8].

When comparing (Fig. 12b) non-ferrous materials with similar electromagnetic properties (brass and bronze), a similar situation occurs. The difference in the amplitude spectrum increases with increasing frequency. The difference in the phase spectra decreases with increasing frequency. The phase difference at lower magnitudes (corresponding to lower frequencies) is equal to about 1.5 degree and only to about 0.25 degree for higher magnitudes (corresponding to higher frequencies). The trend of the phase shift depends on the value of the response parameter α. The response parameter α value of brass is approx. twice greater than that of bronze. It leads to a smaller change in the phase. The change of the phase shift between materials with similar properties is decreasing with decreasing diameter similarly for ferrous and non-ferrous materials.

3.4. Classification

The classification of all measured objects was performed in MATLAB, extended by the pattern recognition toolbox PRTools. A *Support Vector Machine classifier* (SVC) together with *Naive Bayes* (naivebc), *k-Nearest Neighbours* (KNN) and *Linear Nearest Mean Classifier* (NMC) have been used. More details about these classifiers can be found in [20]. Nearest Mean Classifier

is a commonly used classifier and it is primarily used for comparison of classification results. In the paper, the main emphasis is put on the sinc signal only.

To ensure the correct classification of data, a great amount of data has to be collected and processed. To reduce the required volume of data and calculations, the decision has been made that the length of one measurement is 250 k samples. A sample rate of 1 MS/s has been used, i.e. one measurement has taken 250 ms and consisted of 250 periods (1000 samples/period) for each target. At first, raw data have to be filtered. Since the frequency of measured data is from $f_d = 1$ kHz to $f_h = 21$ kHz, a band-pass digital filter has been used. While the measured data from a specific object were compared with the data without any object, the background signal (caused only by the mutual inductance L_{1-2}, no object present) was measured before every single set of measurements. Thereafter, a discrete Fourier transformation was calculated from the filtered raw data of each set and all targets and saved to datasets.

All datasets were stored in a structure consisting of 80 sets of measurements, where one set of measurements contained 20 different samples. Using the algorithm, a set of 10 desired frequencies and corresponding 10 values of amplitude spectra and 10 values of phase spectra different for each sphere and every measurement, were obtained. This way of processing gave a 20-dimensional space (10 amplitudes and 10 phases) for classification. Since classifiers (SVC, naivebc, KNN and NMC) with supervised learning were used, the experimental data arranged in the structure had to be divided into a training data group and a testing data group [24]. There are many papers dealing with an optimal number of training data. One of the proposed methods uses the Learning curve [25]. An optimal size of training data can be determined from the maximum of the Learning curve. The number of training datasets is optimal for 24 sets of measurements out of 80 sets of measurements in total.

3.4.1. Classification into Ferrous and Non-ferrous Materials

Significant differences between ferrous and non-ferrous materials have been shown in Section 3. Multiple frequencies and the fact that ferrous materials increase the induced voltage values and non-ferrous (at higher frequencies) decrease them, together with the induced voltage phase change, lead to the outcome that the classification can be done only by using 20 elemental features (10 magnitudes and 10 phases; *i.e.* solving a 20-dimensional problem). Therefore, the classifier can be trained with corresponding magnitudes and phases, using 24 training datasets, and tested on the rest of 56 datasets. The classifiers are SVC, KNNC with an optimized number of neighbours using the leave-one-out error, NMC and naivebc. The results of classification into two main classes, ferrous and non-ferrous materials, are presented in Table 3.

Table 3. Comparison of all classifiers and their success rates (in %) of classifying into ferrous and non-ferrous classes.

Classifier	**SVC**	**KNNC**	**NMC**	**naivebc**
Poly-harmonic sinc approach	100%	100%	94.4%	97.3%
Classical single-tone method	96.9%	98.5%	94.7%	95.7%

It is evident from these classifying results that, if the multiple frequency approach is used, there is 100% chance of distinguishing ferrous and non-ferrous materials if SVC is used, comparing with classical single-tone methods where the classification success is less than 97%. It can be noticed that KNNC gives good classification results for a laboratory experiment where the measured data are similar, but in the real conditions, where *e.g.* the ground effects have to be

taken into account, KNNC cannot be used because its algorithm is not robust. KNNC classifier is presented only for comparison of results.

3.4.2. Classification into Individual Non-ferrous Materials

There are only slight differences between individual non-ferrous materials, especially for small diameters. In order to classify them into individual material classes, a more complex approach and additional features have to be considered. Magnitudes and phases, together with additional features based on the relations between magnitudes and phases, should be used as features. The added features do not need to have any physical nature and they can be defined using the existing features. To improve the classification, the ratio of magnitudes and phases of each of 10 investigating frequencies were added, together with the differences between two subsequent values of phases (9 features). It adds 19 new features (39 features in total) that improve the separation of individual ferrous and non-ferrous objects. These features were selected based on the results presented in Section 3. Table 4 shows a comparison of results for various numbers of features and for used classifiers.

Table 4. Comparison of all classifiers and their success rates (in %) of classifying into individual non-ferrous classes.

Classifier	SVC	KNNC	NMC	naivebc
Poly-harmonic sinc approach with added features (39 features)	91.3%	99.3%	50%	90%
Poly-harmonic sinc approach (20 elemental features)	89.5%	99.3%	50%	90%
Classical single-tone method	68.2%	91.6%	70.5%	66.3%

The comparison of results shows that the success of SVC is less than 70% if a standard single-tone method is applied. If 20 elementary features are used, the classification success increases to 89.5%. The classification success increases again to 91.3% when all 39 features are used. However, It does not mean that with the increasing number of features (dimensionality) the error rate will be decreasing permanently [26].

3.4.3. Classification into Individual Ferrous Materials

The classification of individual ferrous materials has been done using the same approach as in the classification of non-ferrous materials. Due to small differences between individual materials, additional features used for classification have been added. Table 5 shows results for all tested classifiers and for various numbers of features.

Table 5. Comparison of all classifiers and their success rates (in %) of classifying into individual ferrous classes.

Classifier	SVC	KNNC	NMC	naivebc
Poly-harmonic sinc approach with added features (39 features)	97.3%	99.3%	54.5%	86.2%
Poly-harmonic sinc approach (20 elemental features)	94.4%	100%	50%	85.9%
Classical single-tone method	66.9%	86.1%	75%	78.3%

The results show a similar trend as in the classifying non-ferrous materials. In the case of using only two features (a standard single-tone method), the SVC success rate was smaller than 67%. When 20 elemental features of 10 investigating frequencies were used for classification, the

success rate increased to 94.42%. It confirms the previous results showing that when extra features for classification are added, even better results can be achieved. The classification success increased to 97.32% when all defined features (39) were used. KNNC shows that an increasing number of features does not always decrease the error rate.

3.4.4. Classification into object size classes

The size estimation of a detected object could be considered as another possible classification. It is almost impossible to identify the exact size of a target, but one can roughly estimate a size using different trends of magnitude and phase spectra. The classification into different size estimation classes has been done after a successful classification into individual ferrous and non-ferrous material classes. Since spheres of a diameter ranging from $d = 10$ mm to $d = 25$ mm were used during the experiment, three different classification classes have been chosen. The first class includes object sizes to 10 mm, the second class includes object sizes from 11 mm to 19 mm and third class includes objects larger than 19 mm. To determine the size, an approximate distance from the located object should be known. In [27] or [28], it is shown how to estimate the depth of a located object. The results presented in Table 6 concern the similar distance from the detector head. It is possible to roughly estimate a located ferrous or non-ferrous object size under a given condition. However, as the approximate distance of the object is not always known, it can only be used in certain cases.

Table 6. Comparison of various classifiers and their success rates (in %) of classifying for different sizes of materials.

Classifier		**SVC**	**KNNC**	**NMC**	**naivebc**
Non-ferrous	*Poly-harmonic sinc approach*	100%	100%	85.9%	100%
	Classical single-tone method	98.3%	99.2%	87.5%	92.3%
Ferrous	*Poly-harmonic sinc approach*	99.6%	99.6%	88.8%	100%
	Classical single-tone method	99.3%	99.5%	97.5%	98.8%

4. Conclusion

In the paper, the application of poly-harmonic signals to metal detection and its classification is presented. Step sweep sine-wave, linear frequency sweep and sinc signals were examined. A standard single-tone method offers the greatest sensitivity owing to the possibility of applying a synchronous demodulator. Special synchronous demodulators offer a signal to noise ratio of up to 120 dB, when compared with the poly-harmonic signal method where the synchronous demodulation cannot be performed. Weaknesses of single-tone methods can be found in the fact that the received information about a detected object is contained only in the phase shift. Therefore, measuring only a single phase is not sufficient to state whether the object is ferrous or non-ferrous, or even to state what type of material it is made of. Opposite to single-tone signals, the poly-harmonic signals have to be digitized. The signal-to-noise ratio of such a measurement chain, composed of a preamplifier and an analogue-to-digital converter, does not usually reach more than 90 dB. A detailed analysis is presented in [29].

The frequency step sweep signal confirms the behaviour of ferrous and non-ferrous materials for different frequencies. The experiments show the possibility of using poly-harmonic signals

to measure the response function of a detected object and to use the response function to identify the object. A disadvantage of the frequency step sweep signal is the necessity to use the synchronous demodulation for every frequency separately. The signal is processed per every single frequency, which makes individual measurements time-consuming. A poly-harmonic linear frequency sweep signal covers a wide frequency range of the response function at once. An advantage of this signal is the possibility of this method to display a wider response function when an object is detected. However, the most promising and versatile excitation signal is a sinc signal. It is faster to apply a sinc signal than the other two methods, since all frequencies are generated at once. Furthermore, the number of carrier frequencies and their positions (the start and stop frequencies) can be defined easily.

A support vector classifier was used for the classification of measured data primarily, together with other classifiers. All results showed that if the multiple frequencies' approach (its magnitudes and phases) was used as the features for classification and new features (relations between the existing ones) were added, a successful classification could be obtained.

In the future work, a feature selection will be performed in order to reduce the dimensionality and to select the most relevant features. Several feature selection algorithms, *e.g.* Branch and Bound or Pudil's floating feature selection, has been already tested and it is going to be a part of another project. *Non-destructive testing* (NDT) is another interesting area, where eddy-current methods are used. These techniques used in NDT could be examined and implemented in modern metal detectors, to improve their abilities in a different way.

Acknowledgements

This research was supported by the SGS16/171/OHK3/2T/13 grant provided by the Grant Agency of the Czech Technical University in Prague.

References

[1] Acheroy, N., Milisavljević, M. (2007). Signal processing for humanitarian mine action. *IEEE Signal Process. Mag.*, 24(4), 134–136.

[2] Nováček, P., Roháč, J., Šimánek, J., Ripka, P. (2013). Metal detector signal imprints of detected objects. *IEEE Trans. Magn.*, 49(1), 69–72.

[3] Connor, M., Scott, D.D. (1998). Metal Detector Use in Archaeology: An Introduction. *Hist. Archaeol.*, 34(4), 76–85.

[4] Brooks, J.W. (2000). *The Detection of Buried Non-Metallic Anti-Personnel Land Mines*. The University of Alabama in Huntsville.

[5] Guelle, D., Smith, A., Lewis, A., Bloodworth, T. (2003). *Metal detector handbook for humanitarian demining*. Luxembourg: Luxembourg: Office for Official Publications of the European Communities.

[6] Bielecki, Z., Janucki, J., Kawalec, A., Mikolajczyk, J., Palka, N., Pasternak, M., Pustelny, T., Stacewicz, T., Wojtas, J. (2012). Sensors and systems for the detection of explosive devices – An overview. *Metrol. Meas. Syst.*, 19(1), 3–28.

[7] Candy, B. (2010). Metal Detector Basics and Theory, *Minleab*. Available: *http://www.minelab.com/_files/f/11043/kba_metal_detector_basics_&_theory.pdf.*

[8] Bruschini, C. (2002). *A Multidisciplinary Analysis of Frequency Domain Metal Detectors for Humanitarian Demining*. Vrije Universiteit Brussel, 2002.

[9] Svatoš, J., Vedral, J., Fexa, P. (2011). Metal detector excited by frequency-swept signal. *Metrol. Meas. Syst.*, 18(1), 57–68.

[10] Gao, J., *et al*. (2009). Simulation analysis of multi-frequency eddy current sensor impedance property. *2009 International Conference on Information Engineering and Computer Science*, Wuhan, 1–4.

[11] Brojboiu, M., Popa, I.C., Ivanov, V. (2016). Numerical modeling of an eddy current sensor used in a metal separation device. *2016 International Conference on Applied and Theoretical Electricity*, Craiova, 1–6.

[12] OToole, M., Karimian, N., Peyton, A.J. (2018). Classification of Non-ferrous Metals using Magnetic Induction Spectroscopy. *IEEE Transactions on Industrial Informatics*, 3203, 1–9.

[13] Grant, F.S., West, G.F. (1965). *Interpretation Theory in Applied Geophysics*. New York: McGrawHill.

[14] Svatos, J., Vedral, J. (2012). The Usage of Frequency Swept Signals for Metal Detection. *IEEE Trans. Magn.*, 48(4), 1501–1504.

[15] Svatos, J., Vedral, J., Novacek, P. (2012). Metal object detection and discrimination using Sinc signal. *13th Biennial Baltic Electronics Conference*, 307–310.

[16] Siegenfeld, A. (2003). *ATMID – Technologie und Schaltungsbeschreibung*. Schiebel.

[17] Schiebel, (2002). *ATMID Maintenance Manual*. Schiebel.

[18] Bruschini, C. (2004). On the low-frequency EMI response of coincident loops over a conductive and permeable soil and corresponding background reduction schemes. *IEEE Trans. Geosci. Remote Sens.*, 42(8), 1706–1719.

[19] Matlab Pattern Recognition Toolbox. Delft University of Technology. *http//:prtools.org.* (Sep. 2014).

[20] Svatoš, J., Vedral, J., Fexa, P. (2009). Methods for economical test of dynamic parameters adcs. *Metrol. Meas. Syst.*, 16(1), 161–170.

[21] Kowalewski, M., Lentka, G. (2013). Fast High-Impedance Spectroscopy Method Using Sinc Signal Excitation. *Metrol. Meas. Syst.*, 20(4), 645–654.

[22] Vedral, J., Fexa, P. (2012). DAC testing using impulse signals. *Metrol. Meas. Syst.*, 19(1), 105–114.

[23] van der Heijden, F., Duin, R.P.W., de Ridder, D., Tax, D.M.J. (2004). *Classification, Parameter Estimation and State Estimation*. John Wiley & Sons, Ltd.

[24] Xiao, L., Deng, L. (2010). A geometric perspective of large-margin training of Gaussian models. *IEEE Signal Process. Mag.*, 27(6), 118–23.

[25] Beleites, C., Neugebauer, U., Bocklitz, T., Krafft, C., Popp, J. (2013). Sample size planning for classification models. *Anal. Chim. Acta*, 760, 25–33.

[26] Kaski, J., Peltonen, S. (2011). Dimensionality reduction for data visualization. *IEEE Signal Process. Mag.*, 28(1), 100–104.

[27] Das, Y., McFee, J., Chesney, R. (1985). Determination of Depth of Shallowly Buried Objects by Electromagnetic Induction. *IEEE Trans. Geosci. Remote Sens.*, GE-23(1), 60–66.

[28] Das, Y., McFee, J., Toews, J., Stuart, G.C. (1990). Analysis of an electromagnetic induction detector for real-time location of buried objects. *IEEE Trans. Geosci. Remote Sens.*, 28(3), 278–288.

[29] Svatoš, J. (2015). *Advanced Instrumentation for Polyharmonic Metal Detectors* (Doctoral dissertation), CTU in Prague, Prague, Czechia, *https://dspace.cvut.cz/handle/10467/61084*.